JOURNAL OF SOLID STATE CHEMISTRY 115, 274–282 (1995)

A TEM and XRD Study of $(BiS)_{1+\delta}(Nb_{1+\varepsilon}S_2)_n$ Misfit Layer Structures

L. C. Otero-Diaz, R. L. Withers,*,[1] A. Gomez-Herrero, T. R. Welberry,* and S. Schmid*

*Departamento Quimica Inorganica, Facultad Quimicas, Universidad Complutense, 28040 Madrid, Spain; and *Research School of Chemistry, Australian National University, Canberra, A.C.T. 0200, Australia*

Received June 24, 1994; accepted August 18, 1994

Monolayer and bilayer lamellar misfit layered chalcogenides within the BiS–NbS_2 system have been synthesized and studied via TEM and XRD. Both BiS and NbS_2 parent substructures are shown to have very close to orthorhombic symmetry in the former case, but definite monoclinic symmetry in the latter. Stacking disorder and its effect upon electron diffraction patterns is investigated via higher order Laue zone (HOLZ) diffraction. In addition to the usual set of reflections for such systems, an additional set of weak, somewhat diffuse satellite reflections (not previously reported before for any other misfit layered chalcogenide) have been observed. Bilayer tubular crystals have also been studied by XRD. A close relationship with the corresponding lamellar bilayer phase is established, and some unusual features of its reciprocal lattice are pointed out. © 1995 Academic Press, Inc.

1. INTRODUCTION

A broad range of mineral and synthetic inorganic materials can be classified as misfit layer structures, i.e., composite materials built out of alternating layers or slabs of different structure types (1, 2). Among this class of materials, much attention has very recently been paid to misfit layered chalcogenides of general stoichiometry $(MX)_{1+\delta}(T_{1+\varepsilon}X_2)_n$, where M = any lanthanide (Ln), Pb, Bi, or Sn; T = Ti, V, Cr, Nb, or Ta; and X = S or Se (see, for example, (3) and references contained therein). These misfit compounds are built from alternating layers of MX (a pseudotetragonal two atom thick {100} layer of B1-type) and slabs n layers thick of TX_2 (a pseudohexagonal three atom thick layer of the type found for the corresponding layered transition metal dichalcogenides or TMDs). The prototype phase for this class of misfit layered chalcogenides is monolayer (n = 1) $La_{1.2}CrS_{3.2}$ (4–7).

The resultant composite crystal structures are most elegantly described in terms of the intergrowth of two, often mutually incommensurable, substructures: a pseudotetragonal (so-called Q) substructure based upon the MX layers and a pseudohexagonal (so-called H) substructure based upon the TX_2 slabs. These two substructures have identical b and c (the stacking direction) unit cell parameters, but a axis unit cell parameters which are mutually incommensurable—although typically with a ratio a_H/a_Q close to the ideal of $1/\sqrt{3}$, i.e., ~0.58. The misfit between the two component parts of the structure leads to the general stoichiometry given above with δ dependent upon the relative size of the M and T cations. When the individual TX_2 slabs of the structure consist of more than one TX_2 layer in thickness, the possibility of polytypism and of the incorporation of excess T cations in the van der Waal's gap between the individual TX_2 layers arises, just as for the layered TMDs themselves. This possibility of excess T cations has been incorporated into the above general stoichiometry in the form of the $(T)_{n\varepsilon}$ component. For n = 1, one would except ε = 0, whereas for $n > 1$, ε is not necessarily zero.

In the case of misfit layer structures within the ternary Bi–Nb–S system rather little is known to date (1–3). Gotoh *et al.* (8) have reported the preparation of monolayer (n = 1) misfit compounds for M = Bi; T = Ti, V, Nb, Ta; and X = S, Se from mixtures of the simple elements, in vacuum sealed silica tubes heated up to 800°C. Structural characterization, however, was limited to the observation by X-ray powder diffraction (XRPD) of some 00l reflections. Matsuura *et al.* (9), on the other hand, have reported the preparation of single crystals grown by chemical vapor transport. Again, however, only 00l-type XRPD data were reported. In addition to these preliminary results on the monolayer (n = 1) phase, Oosawa *et al.* (10) have also reported the preparation (again via direct heating of the elements in a vacuum sealed silica tube) of the bilayer (n = 2) phase.

The purpose of this paper is to present new results concerning the preparation and structural characterization (via TEM and XRD) of lamellar and tubular misfit layer structures within the Bi–Nb–S system.

[1] To whom correspondence should be addressed.

0022-4596/95 $6.00

2. EXPERIMENTAL METHODS

2.1. Sample Preparation

A sample with nominal composition $BiNb_2S_5$ was prepared from an appropriate mixture of Bi_2S_3 (5 *N*, Hudson Lab., U.S.A.), Nb (99.9%, Ventron, U.S.A.), and S (5 *N*, American Smelting and Refining Co., NY); 12% of S in excess was used in order to facilitate the reaction. The ground mixture was heated in a vacuum sealed silica tube (20 cm in length and with an internal diameter of 11 mm). The heat treatment given was as follows: 5 days at 400°C, 2 days at 650°C, 14 days at 900°C, followed by slow cooling to room temperature over 9 days at the rate of 100° per day. The obtained product contained a great number of lamellar and tubular "crystals" as well as a blackish-gray microcrystalline powder. The products all showed metallic luster.

2.2. Diffraction Studies

The sample was examined by X-ray powder diffraction (XRPD) using a Siemens K 810 diffractometer (Cu $K\alpha$ radiation) and a D-501 goniometer with a secondary graphite monochromator. Si (5 *N*) was used as an internal standard. Good single crystals of the lamellar bilayer ($n = 2$) phase were extracted from the reaction products and the corresponding unit cell parameters determined from single crystal data obtained using a Philips PW 1100/20 diffractometer equipped with a graphite monochromator.

Rotation-photograph-like pictures of the tubular crystals were obtained using a single stationary crystal exposure (Cu $K\alpha$ radiation) with the X-ray beam perpendicular to the cylindrical axis (for some discussion on the scattering geometry used and the crystallography of cylindrical "crystals" see, for example, the discussion on Chrysotile given on pp. 282–285 of (11)). To explore the variation of scattering with crystal orientation, use was also made of a position sensitive detector Weissenberg system (described in (12)) which allowed whole reciprocal lattice sections to be recorded.

SEM studies were carried out using a JEM 6400 SEM operating at 20 kV and fitted with a Lynk 10000 analyzer system. Samples for TEM observation were obtained from solutions ultrasonically dispersed under butanol; one drop of the solution was placed on Cu grids coated with holey Carbon support films. The resultant TEM specimens were subsequently examined in JEOL 100CX and 2000FX electron microscopes.

3. RESULTS

3.1. SEM Studies

Sample observation by SEM shows at least three distinct types of crystal morphology:

(a) Lamellar crystals of variable size but up to ~0.5 cm^2 in area. Some of them are bent and they often appear forming aggregates (see Fig. 1a). Semiquantitative XEDS, using Bi_3TiNbO_9 as a standard, gave somewhat variable results (although typical with Bi/Nb ratios of either ~1.1 or ~0.5), suggesting the presence of both monolayer and bilayer lamellar crystals. This was subsequently confirmed by TEM and XRPD results.

(b) Cylindrically shaped "crystals" in the form of holey tubes (see Fig. 1b) up to 1 mm in length and ~0.1 mm in external diameter. Similarly shaped crystals have also been reported to occur in the Pb–Nb–S system (13). Electron microprobe analysis in this latter case suggested a composition of $\sim PbNb_2S_5$. Semiquantitative XEDS results in our case give a Bi/Nb ratio ~0.5, likewise suggesting a composition of $\sim BiNb_2S_5$.

(c) Prismatic crystals up to 100 μm in length and ~0.1 μm in width which often appear decorating the surfaces of both the lamellar and tubular crystals (see Fig. 1b). XEDS from these crystals reveals only the characteristic lines ($K\alpha$, $K\beta$, and L) of Nb and O so that these crystals correspond to Nb_2O_5. There are at least five distinct polymorphs of Nb_2O_5 (14) known. By TEM, the prismatic crystals were identified as the tetragonal M–Nb_2O_5 polymorph. A few grains of the monoclinic H–Nb_2O_5 polymorph as well as of the 3R polymorph of NbS_2 and of unreacted starting product Bi_2S_3 were also found via TEM. These phases, however, constituted only a minor portion of the final reaction products.

3.2. Powder X-Ray Diffraction Results

The X-ray powder pattern from the bulk sample was complex with many maxima (up to 57) observed in the range $5° < 2\theta < 90°$, suggesting the probable presence of several phases. This was confirmed by electron diffraction from single grains, and the indexing of these latter electron diffraction patterns (EDPs) necessarily preceded the indexing of the bulk X-ray powder pattern. The XRPD data simply enable unit cell parameters to be refined once the approximate unit cell size has been determined by electron diffraction.

Unit cell parameters have been obtained for both the monolayer ($n = 1$) and bilayer ($n = 2$) ternary phases and are listed in Table 1 along with the corresponding b/a ratios. The deviation of these latter parameters from the ideal values of 1 and $\sqrt{3}$, respectively, gives a measure of the probability of the presence of orientational variants of one or other substructure (15, 16). The distortions of the H and Q substructures away from ideal hexagonality and tetragonality, respectively, were more or less the same for both the monolayer and bilayer phases. The majority lamellar phase was the bilayer ($n = 2$) phase. Lines that might be due to the cylindrical phase were difficult to unambiguously identify.

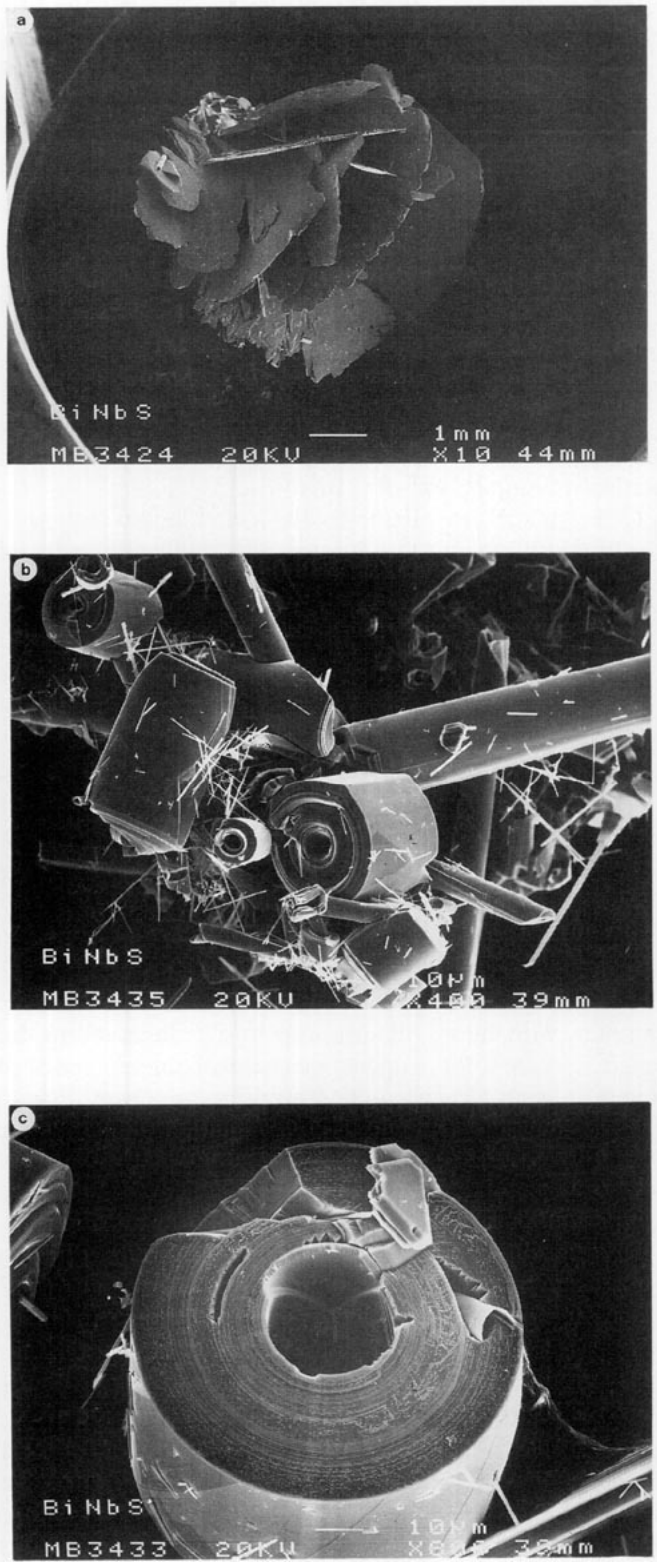

FIG. 1. Scanning electron micrographs of the as prepared specimen showing (a) a typical lamellar aggregate, (b) the cylindrically shaped "crystals" in the form of holey tubes, and (c) an example of a particularly well-ordered tubular crystal. Note the much smaller scale prismatic crystals decorating the surface of the tubular crystals in (b).

3.3. Single Crystal X-Ray Diffraction of Lamellar Crystals

A range of lamellar crystals were investigated for their suitability for a single crystal X-ray diffraction study. Some suitable bilayer (n = 2) crystals were found and their unit cell parameters determined. The results were in close agreement with those obtained via XRPD. A single crystal X-ray structure refinement is underway (although this is complicated by the presence of somewhat diffuse satellite reflections in addition to those that might have been expected) and the results will be presented elsewhere.

3.4. "Single Crystal" X-Ray Diffraction of the Tubular Crystals

The type and extent of ordering involved in the tubular "crystals," because of their morphology, is rather difficult to study via either electron diffraction or conventional X-ray diffractometry. Nonetheless some information has been obtained from an apparently extremely well-ordered tubular crystal (see Fig. 1c) via X-ray rotation-photograph-like pictures taken with the X-ray beam perpendicular to the cylindrical axis (see Fig. 2). Well-defined $(00l)^*$ and $(0kl)^*$ type reflections are observed (in the zero layer level up to l = 21). The corresponding b and c axis dimensions of ~5.80 and 17.44 Å, respectively, confirms that the radial direction of the tube is the stacking direction and suggests a close relationship between the lamellar and tubular phases.

Such dimensions are virtually identical to those obtained for the lamellar bilayer phase (see Table 1). Indeed

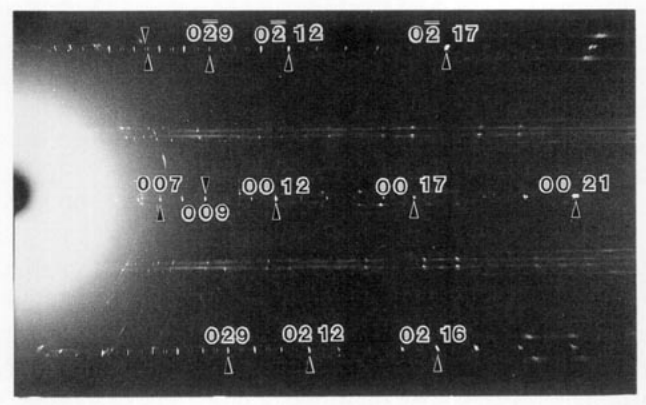

FIG. 2. X-ray rotation-photograph-like picture of a well-ordered tubular "crystal" obtained using a single stationary crystal exposure (Cu $K\alpha$ radiation) with the X-ray beam perpendicular to the cylindrical axis. Note the presence of weak satellite reflections (arrowed) characterized by a modulation wave-vector $\mathbf{q}$ ~0.41$\mathbf{c}^*$ and the quite strong satellite reflections, as well as more or less continuous diffuse streaking at upper layer levels separated from the parent $k = -2\mathbf{b}^*$, $0\mathbf{b}^*$, and $+2\mathbf{b}^*$ levels by multiples of ~0.163 Å^{-1}, i.e., ~0.945$\mathbf{b}^*$.

the resemblance is even more striking in that the angle between **b** and **c**, α, is also ~93°, as can be derived from the offset of the circular rings corresponding to $(00l)^*$ and $(0kl)^*$ type reflections in the $k = 0$ and $k = 2$ levels of reciprocal space shown in Fig. 3. Note that scattering comes from only one side of the cylinder as a result of absorption, i.e., reflections are obtained from one side only of each possible set of $0kl$ planes. Reflections from the reverse side of these planes would involve transmission through the bulk of the sample. Consequently the radii of the rings in the lower portion of Fig. 3 appear larger than in the upper portion. These rings correspond to planes such as 029, etc., as seen on the rotation-like photograph of Fig. 2. Rings due to reflections such as 0, 2, -9 which would have smaller radii than 009 have been removed by absorption.

It seems sensible to suggest that holey tube morphology must occur as a result of the growth, in an appropriately curved fashion, of thin plates (consisting perhaps of one or more basic units made up of one BiS layer in conjection with a NbS_2 layer on either side) perpendicular to the lamellar c direction which eventually curl up inside one another in a helical or yule-log-like fashion. The relative siting of these curved thin planes (perpendicular to the lamellar **c** direction) from one to the next along the radial direction of the holey tubes would then depend upon the interaction of successive NbS_2 layers across a nominal van der Waal's gap. Consequently one might expect the resultant holey tube "crystals" to exhibit little correlation in the relative siting of the curved thin planes from one to the next along the radial direction of the holey tubes but extensive order perpendicular to this radial direction. The apparent absence of any other type of reflections apart from the $(00l)^*$'s in the zero level of the rotation photograph is consistent with such a view. The existence of well-defined upper layer levels, however, is not and suggests that lattice planes perpendicular to the holey tube axis remain well defined.

In addition, however, there remain several further intriguing features of Fig. 2 that were unexpected. The first

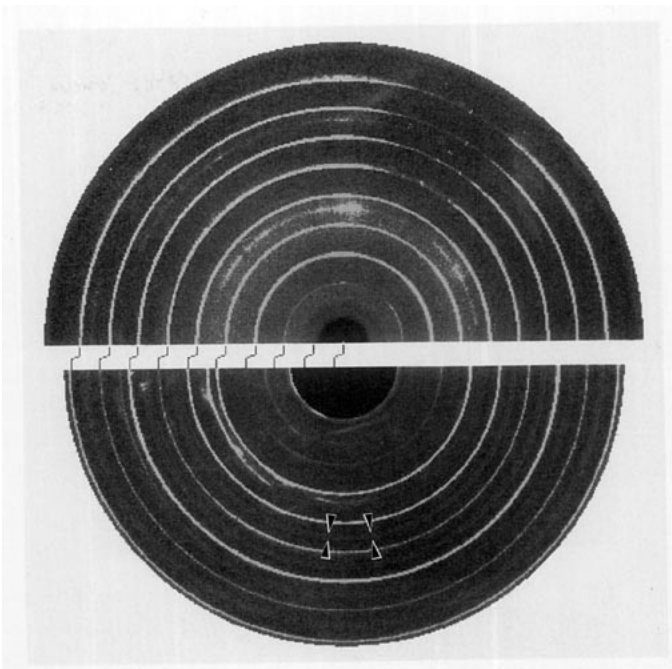

FIG. 3. The top portion of the figure shows the $k = 0$ level of reciprocal space, while the lower portion shows the $k = 2$ portion. The outermost ring in the lower portion corresponds to the 029 reflection. Note the offset between the $00l$ and $02l$ rings in the two sections and the presence of weak satellite rings characterized by a modulation wave-vector $\mathbf{q} \sim 0.41\mathbf{c}^*$ (arrowed) in the $k = 2$ portion.

is the presence of quite strong satellite reflections as well as more or less continuous diffuse streaking at upper layer levels separated from the parent $k = -2\mathbf{b}^*$, $0\mathbf{b}^*$, and $+2\mathbf{b}^*$ levels by multiples of ~0.163 Å^{-1}, i.e., ~$0.945\mathbf{b}^*$. Our first thought was that what we have labelled the $\mathbf{b}^*$ direction must in fact correspond to the bilayer $\mathbf{a}_\delta^*$ direction of reciprocal space so that these additional upper layer level reflections could be interpreted as arising from the H substructure. The measured reciprocal lattice dimension of ~0.163 Å^{-1}, i.e., ~$0.945\mathbf{b}^*$ corresponding to this additional modulation, however, is not compatible with such an interpretation. The existence of these upper layer levels must then imply the existence of some sort of incommensurate modulation of the lattice planes perpendicular to the holey tube axis and characterized by a primary modulation wave-vector with a component along the holey tube axis of ~$0.945\mathbf{b}^*$.

The second unexpected feature of Fig. 2 is the presence of weak extra satellite reflections (arrowed in the top left of Fig. 2 but also present in the bottom $k = 2$ portion of Fig. 3 in between the $(02l)^*$ rings) in addition to the $(02l)^*$ and $(0, -2, l)^*$ parent reflections in the $k = 2$ and $k = -2$ upper layer levels. These additional satellite reflections require the existence of a further incommensurate modulation characterized this time by a primary modulation wave-vector ~$0.41\mathbf{c}^*$. The absence of these

TABLE 1
Refined Unit Cell Parameters from X-Ray Powder Diffraction Data

Subsystem	a (Å)	b (Å)	c (Å)	α	β	γ	b/a
The ~$Bi_{1.174}NbS_{3.174}$ monolayer phase							
BiS	5.667(1)	5.790(2)	23.215(5)	90	90	90	1.022
NbS_2	3.3252(8)	5.791(1)	23.232(5)	90	90	90	1.742
The ~$Bi_{1.166}Nb_2S_{5.166}$ bilayer phase (assuming $\varepsilon = 0$)							
BiS	5.682(2)	5.769(1)	17.416(5)	93.26(2)	90	90	1.015
NbS_2	3.313(1)	5.774(1)	17.419(3)	93.15(2)	90	90	1.743

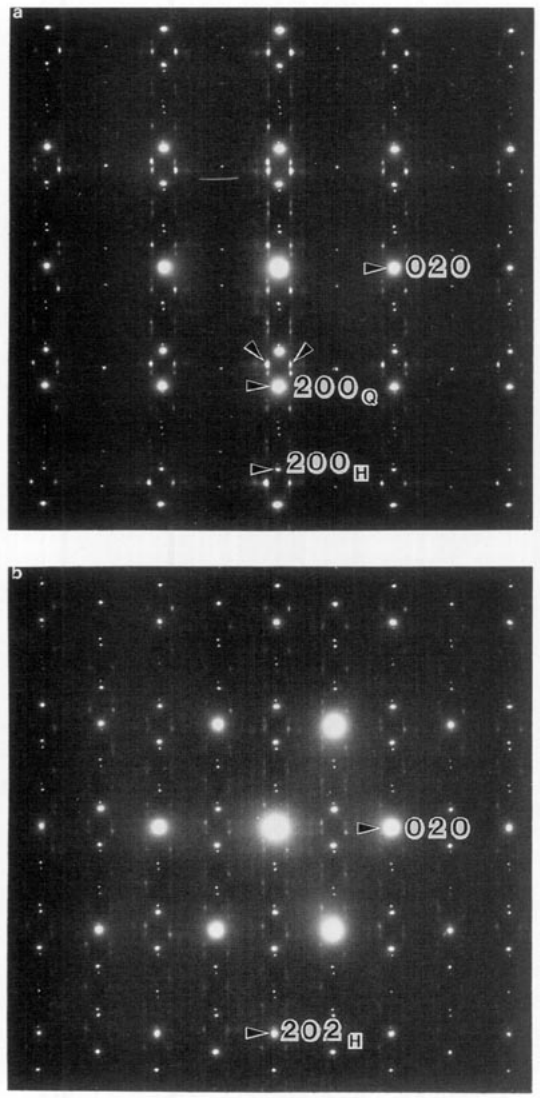

FIG. 4. The ZOLZ regions of SADPs typical of the lamellar $n = 1$ monolayer phase and taken at the (a) [001] and (b) $[-1, 0, 1]_H$ zone axis orientations. The parent substructure reflections are indexed.

additional satellite reflections in the $k = 0$ level implies that the modulation is displacive in origin and must involve atomic displacements along the **b** direction, i.e., along the axis of the holey tube itself. Further consideration of these features, however, is beyond the scope of the current paper. Nonetheless it remains clear that there is still much to be learned about the nature and extent of order in these holey tube type misfit layer compounds.

3.5. TEM Results from the Lamellar Monolayer Phase

Figure 4 shows the central portions (the zero order Laue zone or ZOLZ regions) of selected area electron diffraction patterns (SADPs) typical of the lamellar $n = 1$ monolayer phase and taken at the (a) [001] and (b) [−1, 0, 1]h zone axis orientations. These two zone axis orientations are separated by an ~8.2° rotation about the (020)* reflection common to both substructures. The fact that the lamellar crystals are typically very thin along the stacking direction in conjunction with the shape transform effect means that Q substructure reflections continue to be observed at pure H substructure zone axis orientations such as the $[-1, 0, 1]_H$ zone axis orientation of Fig. 4b.

In addition to the strong set of parent reflections (indexed) corresponding to the underlying Q and H average substructures and the extremely sharp set of weaker satellite reflections corresponding to higher order linear combinations thereof, note the presence of an additional set of weak, somewhat diffuse satellite reflections (arrowed in (a)) characterized by primary modulation wave-vectors $\mathbf{q} \sim 1.63\mathbf{a}_Q^* \pm 0.20\mathbf{b}^*$ (in terms of the Q substructure) $= 0.96\mathbf{a}_H^* \pm 0.20\mathbf{b}^*$ (in terms of the H substructure). A similar set of weak, somewhat diffuse satellite reflections, and characterized by almost identical primary modulation wave-vectors, also occurs in the bilayer SADPs (see Fig. 6 below). Such satellite reflections have not, to the best of our knowledge, been reported before for any misfit layered chalcogenide. They are, however, ubiquitous and always present in each grain of either the monolayer or bilayer phase investigated in this study. The presence of such satellite reflections requires the existence of an additional compositional and/or displacive modulation of either and/or both of the Q and H substructures in addition to the modulation of both induced by mutual incommensurability of their parent substructures. The structural origin of this additional modulation, however, is at this stage obscure. If it were only present in the bilayer phase one might attribute it to ordering of excess Nb atoms in the van der Waal's gap between neighbouring NbS_2 layers. The clear presence of these satellites in the monolayer phase, however, appears to rule out such an interpretation.

The previously reported average structure space group symmetries, as determined by single crystal X-ray diffraction, of both Q and H substructures for monolayer phases with similar cell dimensions to those given in Table 1 (e.g., $(NdS)_{1.18}NbS_2$; see Wiegers and Meerschaut (3) for other examples) is $Fm2m$. Ignoring the existence of the weak, somewhat diffuse satellite reflections described above, the remaining reflections in the [001] zone axis SADP of Fig. 4a are as might be expected except for the very weak presence of $(hk0)_H^*$ reflections for which h and k are not both even, e.g., $(110)_H^*$. Such reflections should be forbidden by $Fm2m$ space group symmetry. Note, however, that the $(hk0)_Q^*$ reflections for which h and k are not both even are extinct as $Fm2m$ average structure space group symmetry would require.

The presence in TEM SADPs of reflections forbidden by single crystal X-ray determined space group symmetries has been a rather puzzling feature of electron diffraction studies of misfit layer chalcogenides to date (15, 16). Kuypers and van Landuyt (16), for example, in a recent review of TEM studies of misfit layered chalcogenides, point out that the Q and H substructures of most monolayer phases appear C-centered rather than F-centerd, i.e., $(hk0)^*_Q$ and $(hk0)^*_H$ reflections for which h and k are not both even are typically always observed in [001] zone axis SADPs (see, for example, Figs. 3–5 of (16)). While the $(hk0)^*_Q$ reflections for which h and k are not both even are typically only weakly present in the reported [001] zone axis SADPs, $(hk0)^*_H$ reflections for which h and k are not both even are reported as being typically strongly present (see, for example, Figs. 3a, 4a, and 5c in (16)).

This is a major contradiction between electron diffraction and single crystal XRD results and has even lead Kuypers and van Landuyt (16) to suggest that "... the systematic shift over **b**/2 of successive TS_2 layers, which gives rise to a face-centered TS_2 sublattice, is not a general structure feature..." of such monolayer phases. They raise the possibility of stacking disorder arising from the four essentially different basic stacking possibilities corresponding to successive layers of each substructure being stacked either vertically one above the other or being displaced relative to the other over $\frac{1}{2}$**b**. Shifts over **b**/2 of successive TS_2 layers are not therefore seen as an essential component of the structure, but rather as translational faults which may or may not be present in significant numbers.

The reported strong presence, in the majority of TEM foils examined, of $(hk0)^*_H$ reflections for which h and k are not both even is taken as implyng that successive layers of each substructure must largely be stacked vertically one above the other with only a small number of **b**/2 translational faults (see p. 254 of (16)). This, however, does not explain the typical absence of such reflections in the single crystal X-ray studies (3). Reflections of this type could obviously be made to weaken considerably were the **b**/2 translational faults rather more common. A considerable amount of such stacking disorder should smear out the corresponding higher order Laue zone, or HOLZ, rings. Experimentally however, at least in our case, the H substructure HOLZ rings are always rather well defined (see Fig. 5). Hence there still seems to be a fundamental contradiction between the TEM and single crystal XRD results.

We believe that the reported strong presence of $(hk0)^*_H$ reflections for which h and k are not both even is not primarily due to translational faulting (although some minor amount of such faulting probably does occur) but rather is a consequence of misindexing $\langle 101\rangle_H$ substructure

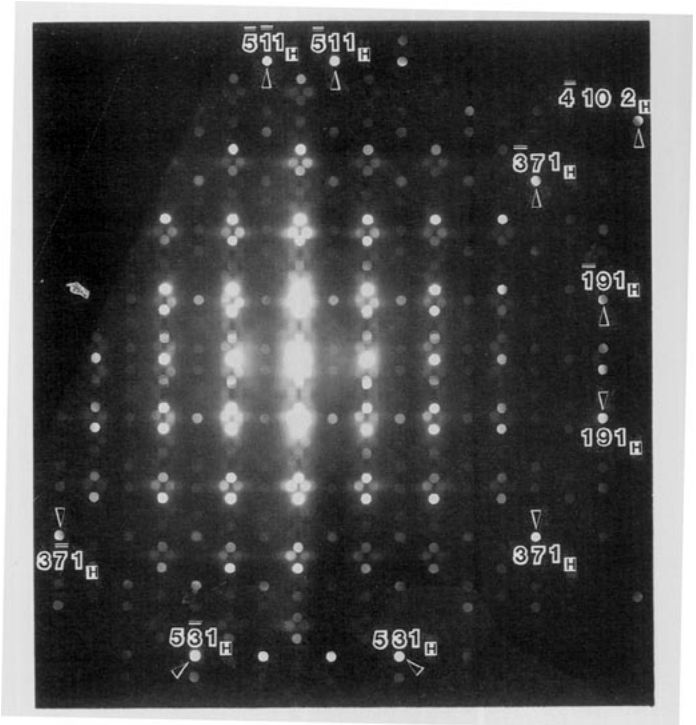

FIG. 5. An [001] zone axis microdiffraction pattern typical of the lamellar $n = 1$ monolayer phase. The indexing of the ZOLZ region is as given in Fig. 4a. The well-defined H substructure HOLZ rings imply that any stacking disorder in the H substructure is minimal.

zone axis SADPs such as that shown in Fig. 4b as [001] zone axis SADPs. This suggestion is prompted by the very close similarity between our Fig. 4b and, for example, Fig. 4c of (16). Note that $|(202)^*_H|/|(200)^*_H| = 1.01$ (using the lattice parameters of Table 1) and hence it is very difficult to distinguish [001] from $\langle 101\rangle_H$ zone axis SADPs based solely upon the position of reflections, particularly if the lattice parameters show slight variability from grain to grain. The presence of a very slight orientational anomaly in Fig. 4a, for example, indicates that the reported lattice parameters in Table 1 need some small adjustment in order to describe the grain from which Fig. 4 was taken. Possible ambiguities in indexing SADPs, however, are helped considerably if HOLZ rings are taken into account.

3.6. TEM Results from the Lamellar Bilayer Phase

Figure 6 shows the central portions (the zero order Laue zone or ZOLZ region) of (a) [001] and (b) $[-1, 1, 2]_H$ zone axis SADPs typical of the lamellar $n = 2$ bilayer phase. Figure 7 shows an [001] zone axis microdiffraction pattern; the FOLZ ring corresponding to the 17.4 Å c dimension is clearly visible. The comments above as to the difficulty in unambiguously indexing SADPs is even more acute in this case. There are quite a few crystallograpically distinct zone axes that give almost identical

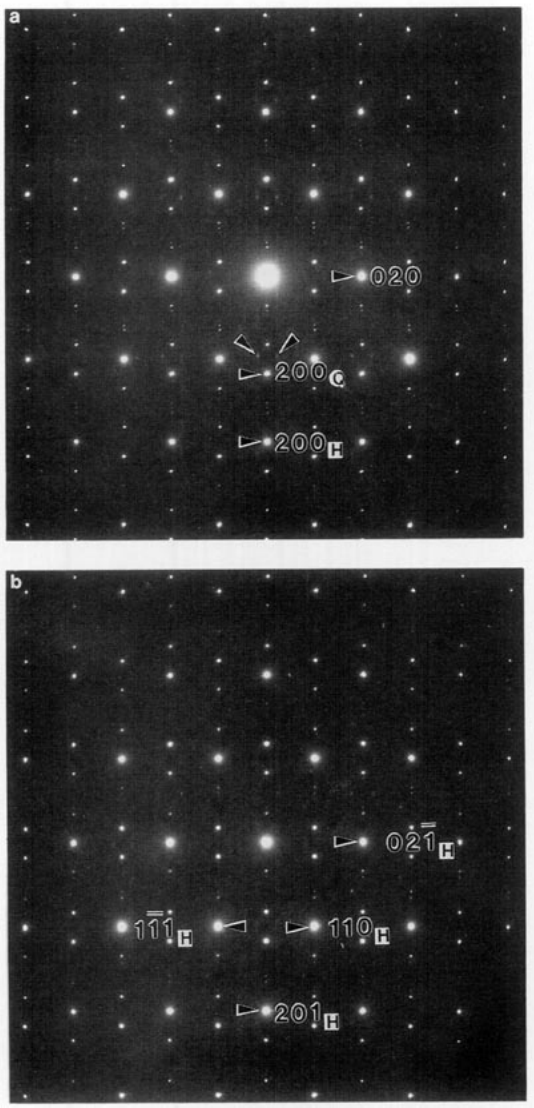

FIG. 6. The ZOLZ region of (a) [001] and (b) $[-1, 1, 2]_H$ zone axis SADPs typical of the lamellar $n = 2$ bilayer phase. The parent Q and H substructure reflections are indexed in (a) and the H substructure reflections in (b).

SADPs that can only be distinguished by very careful measurement (taking into account HOLZ rings) and by systematic tilting experiments. Even so, there still remain slight ambiguities, e.g., $|(200)^*_H|/|(020)^*_H|$ as measured from Fig. 6a is 1.72 instead of the expected 1.74. Nonetheless the pattern as indexed gives the best fit to the cell data of Table 1. It would seem therefore that cell parameters may vary slightly from grain to grain.

Again note the presence of the additional set of weak, somewhat diffuse satellite reflections (arrowed in (a)) and characterized by almost identical primary modulation wave-vectors to those occurring in the monolayer phase. There have to date been relatively few structure refinements of bilayer phases. The only previously reported bilayer structure refinement with similar cell dimensions is that of $(PbS)_{1.18}(TiS_2)_2$ (17). The reported average structure space group symmetries of both Q and H substructures in that case were $C2/m$ and $C2_1/m$, respectively. Certainly the average NbS_2 substructure is C-centered (see Fig. 6). Tilting experiments show that the BiS substructure is likewise C-centered. If it were not for the fact that the Ti's in $(PbS)_{1.18}(TiS_2)_2$ are octahedrally coordinated whereas Nb's in all known misfit layer chalcogenides to date are trigonal prismatically coordinated, it would seem reasonable to assert that the two structures should be isomorphous. The results of a single crystal X-ray study of the bilayer phase are under way and will be reported elsewhere.

Figure 8a shows an ~[100] zone axis SADP and (b) the corresponding HREM image (showing the ~17.4 Å layer spacing along the **c** direction) fortuitously obtained at the edge of a thin foil. The ~87° angle between **b*** and **c*** is clearly visible both in the SADP and the corresponding image. Note that the 0, $2k$, l rows contain sharp reflections (corresponding to a repeat period of ~17.4 Å) connected by weak streaking. However, as was also reported by Kuypers and van Landuyt in the case of $PbNb_2S_5$ (15, 16), there exist heavily streaked 0, $2k + 1$, l rows implying not only stacking disorder but also some violation of C-centering. (No evidence for such a viola-

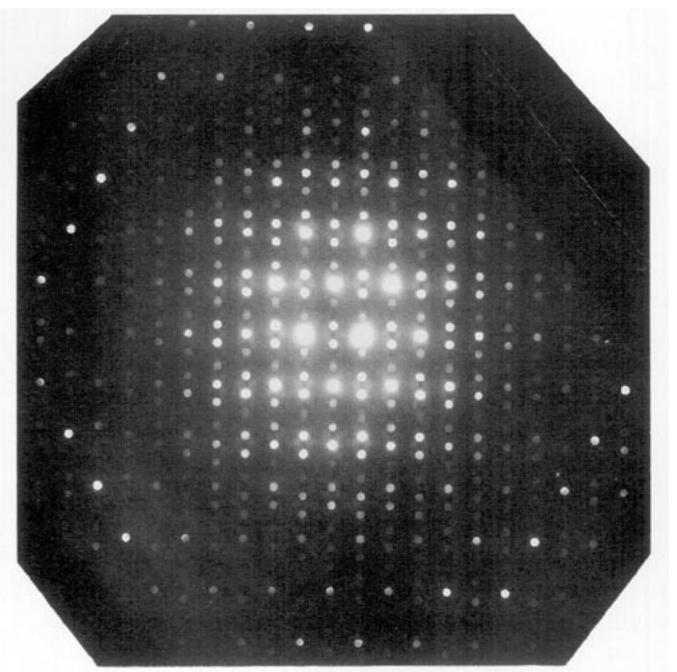

FIG. 7. An [001] zone axis microdiffraction pattern of the lamellar $n = 2$ bilayer phase; the FOLZ ring corresponding to the 17.4 Å dimension is clearly visible. The indexing of the ZOLZ region is as given in Fig. 6a.

tion of C-centering, however, was ever observed in SADPs taken looking approximately perpendicular to the thin foil. Hence it is possible, as also suggested by Kuypers and van Landuyt (16), that this apparent disorder might well be due to deformation of the thin foil at its edge.) The fact that well-defined HOLZ rings can easily be obtained for the NbS_2 subsystem but never for the BiS subsystem suggests that most of the disorder occurs in the BiS subsystem. Kuypers and van Landuyt came to a similar conclusion as regards the PbS subsystem in the case of $PbNb_2S_5$ (15, 16).

3.7. *TEM Results from an Unknown Lamellar Phase*

Finally, we very occasionally came across SADPs of the type shown in Fig. 9. This type of SADP is clearly closely related to the monolayer and bilayer phases but has not yet been properly characterized. Note the usual approximately hexagonal array of reflections corresponding to the pseudohexagonal NbS_2 substructure. Each of the BiS substructure reflections, however, appear to have split into a cluster of reflections. Semiquantitative XEDS gave a Bi : Nb ratio of ~1 : 3, suggesting it comes from a trilayer phase. Unfortunately it has not yet been possible to determine the corresponding **c** axis. To date there have been only a few reports of trilayer phases (18, 19). Attempts to synthesize more phase pure specimens are under way.

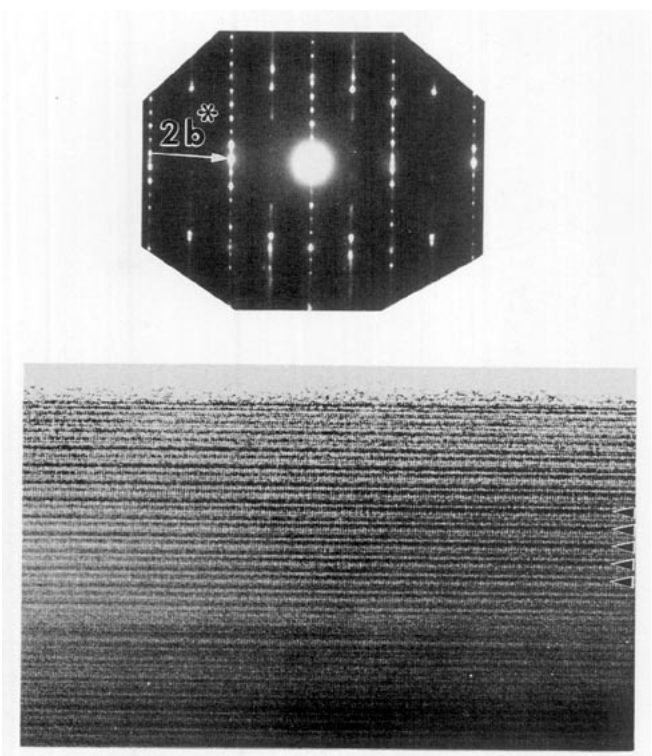

FIG. 8. An ~[100] zone axis SADP (top) and the corresponding HREM image (bottom) The **c*** direction is vertically down the page, while the **2b*** direction is marked on the SADP. Note that the 0, 2*k*, *l* reciprocal rows contain sharp reflections connected by weak streaking. In addition, however, note the heavily streaked 0, 2*k* + 1, *l* rows. The 17.4 Å stacking repeat (arrowed) is clearly visible in the HREM image, as are the ~2.9 Å fringes corresponding to |**b**/2|.

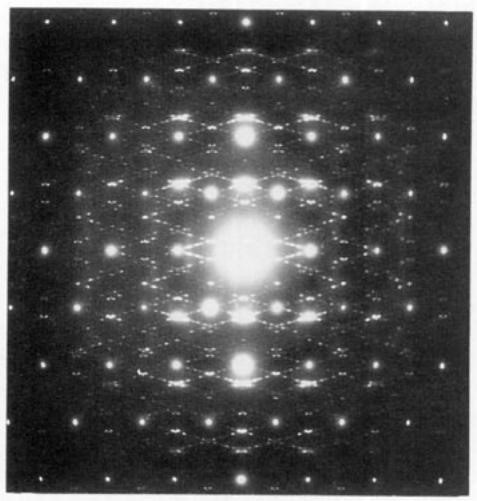

FIG. 9. An extremely complicated SADP occasionally observed. The pseudohexagonal NbS_2 substructure is clearly visible. Each of the BiS substructure reflections, however, appear to have split into a cluster of reflections. The *c* axis dimension is yet to be determined.

4. CONCLUSIONS

In conclusion, both mono- and bilayer lamellar misfit layer structures exist within the BiS–NbS_2 system with cell dimensions and space group symmetries closely related to some previously reported phases (3). The well-defined nature of H substructure HOLZ rings in both the mono- and bilayer lamellar phases suggests that stacking disorder is not a major feature of the H substructure. The origin of the addition set of weak diffuse satellite reflections which occur in both the monolayer and bilayer phases is unclear, as is the detailed relationship between the lamellar and tubular bilayer phases. Despite intensive investigation over recent times, it is clear that there is still much to be learned about misfit layer chalcogenides.

ACKNOWLEDGMENTS

Two of us (L.C.O.-D. and A.G.-H.) thank the Centro de Microscopia Electronica (Universidad Complutense de Madrid) for the use of its facilities. This work was partly supported by CICYT, Project MAT-92-0374.

REFERENCES

1. E. Makovicky and B. G. Hyde, *Struct. Bonding* **46,** 101 (1981).
2. E. Makovicky and B. G. Hyde, *Mater. Sci. Forum* **100–101,** 1 (1992).

3. G. A. Wiegers and A. Meerschaut, *Mater. Sci. Forum* **100–101,** 101 (1992).
4. K. Kato, I. Kawada, and T. Takahashi, *Acta Crystallogr. B* **33,** 3437 (1977).
5. L. C. Otero-Diaz, J. D. Fitz Gerald, T. B. Williams, and B. G. Hyde, *Acta Crystallogr. B* **41,** 405 (1985).
6. T. B. Williams and B. G. Hyde, *Acta Crystallogr. B* **44,** 467 (1988).
7. K. Kato, *Acta Crystallogr. B* **46,** 39 (1990).
8. Y. Gotoh, M. Onoda, K. Uchida, Y. Tanaka, T. Iida, H. Hayakawa, and Y. Oosawa, *Chem. Lett.*, 1559 (1989).
9. K. Matsuura, T. Wada, N. Suzuki, T. Nakamizo, S. Ikegawa, H. Yamauchi, and S. Tanaka, *Jpn. J. Appl. Phys.* **29,** L473 (1990).
10. Y. Oosawa, Y. Gotoh, and M. Onoda, *Chem. Lett.*, 1563 (1989).
11. L. W. Bragg and G. F. Claringbull, "Crystal Structure of Minerals," Vol. IV. G. Bell and Sons, London, 1965.
12. J. C. Osborn and T. R. Welberry, *J. Appl. Crystallogr.* **23,** 476 (1990).
13. L. Guemas, P. Rabu, A. Meerschaut, and J. Rouxel, *Mater. Res. Bull.* **23,** 1061 (1988).
14. B. G. Hyde and S. Andersson, "Inorganic Crystal Structures." Wiley, New York, 1989.
15. S. Kuypers, J. van Landuyt, and S. Amelinckx, *J. Solid State Chem.* **86,** 212 (1990).
16. S. Kuypers and J. van Landuyt, *Mater. Sci. Forum* **100–101,** 223 (1992).
17. A. Meerschaut, C. Auriel, and J. Rouxel, *J. Alloys Compounds* **183,** 129 (1992).
18. Y. Oosawa, Y. Gotoh, J. Akimoto, T. Tsunoda, M. Sohma, and M. Onoda, *Jpn. J. Appl. Phys.* **31,** L1096 (1992).
19. Y. Oosawa, Y. Gotoh, J. Akimoto, M. Sohma, T. Tsunoda, and H. Hayakawa, *Solid State Ionics* **67,** 287 (1994).